

## Accepted Manuscript

Dual Inhibitors of RAF-MEK-ERK and PI3K-PDK1-AKT pathways: Design, Synthesis and Preliminary Anticancer Activity Studies of 3-Substituted-5-(phenylamino) indolone Derivatives

Zutao Yu, Zhuo Chen, Qiongli Su, Shiqi Ye, Hongbo Yuan, Mengni Kuai, Meng Lv, Zhijun Tu, Xiaoping Yang, RangRu Liu, Gaoyun Hu, Qianbin Li

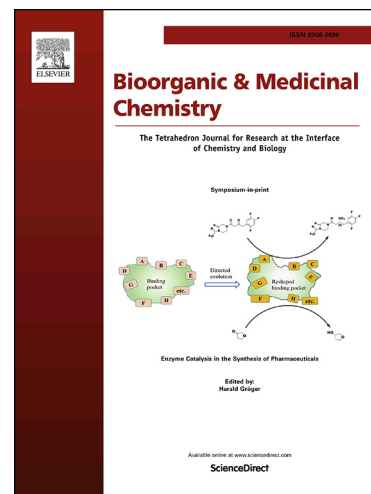
PII: S0968-0896(18)32004-2  
DOI: <https://doi.org/10.1016/j.bmc.2019.01.028>  
Reference: BMC 14720

To appear in: *Bioorganic & Medicinal Chemistry*

Received Date: 25 November 2018  
Revised Date: 21 January 2019  
Accepted Date: 23 January 2019

Please cite this article as: Yu, Z., Chen, Z., Su, Q., Ye, S., Yuan, H., Kuai, M., Lv, M., Tu, Z., Yang, X., Liu, R., Hu, G., Li, Q., Dual Inhibitors of RAF-MEK-ERK and PI3K-PDK1-AKT pathways: Design, Synthesis and Preliminary Anticancer Activity Studies of 3-Substituted-5-(phenylamino) indolone Derivatives, *Bioorganic & Medicinal Chemistry* (2019), doi: <https://doi.org/10.1016/j.bmc.2019.01.028>

This is a PDF file of an unedited manuscript that has been accepted for publication. As a service to our customers we are providing this early version of the manuscript. The manuscript will undergo copyediting, typesetting, and review of the resulting proof before it is published in its final form. Please note that during the production process errors may be discovered which could affect the content, and all legal disclaimers that apply to the journal pertain.



## Dual Inhibitors of RAF-MEK-ERK and PI3K-PDK1-AKT pathways: Design, Synthesis and Preliminary Anticancer Activity Studies of 3- Substituted-5-(phenylamino) indolone Derivatives

Zutao Yu<sup>a</sup>, Zhuo Chen<sup>a</sup>, Qiongli Su<sup>b</sup>, Shiqi Ye<sup>c</sup>, Hongbo Yuan<sup>d</sup>, Mengni Kuai<sup>a,b</sup>, Meng Lv<sup>a</sup>, Zhijun Tu<sup>a</sup>, Xiaoping Yang<sup>b</sup>, RangRu Liu<sup>e</sup>, Gaoyun Hu<sup>a</sup>, Qianbin Li<sup>a\*</sup>

<sup>a</sup> *Department of Medicinal Chemistry, Xiangya School of Pharmaceutical Sciences, Central South University, Changsha 410013, Hunan, P. R. China;*

<sup>b</sup> *Department of Pharmacy, School of Medicine, Hunan Normal University, Changsha 410013, Hunan, P. R. China;*

<sup>c</sup> *School of Medicine, Shenzhen University, Shenzhen 518060, Guangdong, P.R. China;*

<sup>d</sup> *Hunan Qianjin Xiangjiang Pharmaceutical Co.,Ltd, Changsha 410013, Hunan, P. R. China;*

<sup>e</sup> *Key Laboratory of Tropical Diseases and Translational Medicine of the Ministry of Education & Hainan Provincial Key Laboratory of Tropical Medicine, Hainan Medical College, Haikou, China.*

### ABSTRACT

The dysfunction and mutual compensatory activation of RAF-MEK-ERK and PI3K-PDK1-AKT pathways have been demonstrated as the hallmarks in several primary and recurrent cancers. The strategy of concurrent blocking of these two pathways shows clinical merits on effective cancer therapy, such as combinatory treatments and dual-pathway inhibitors. Herein, we report a novel prototype of dual-pathway inhibitors by means of merging the core structural scaffolds of a MEK1 inhibitor and a PDK1 inhibitor. A library of 43 compounds that categorized into three series (Series I-III) was synthesized and tested for antitumor activity in lung cancer cells. The results from structure-activity relationship (SAR) analysis showed the following order of antitumor activity that 3-hydroxy-5-(phenylamino) indolone (Series III) > 3-alkenyl-5-(phenylamino) indolone (Series I) > 3-alkyl-5-(phenylamino) indolone (Series II). A lead compound **9za** in Series III showed most potent antitumor activity with IC<sub>50</sub> value of 1.8±0.8 μM in A549 cells. Moreover, antitumor mechanism study demonstrated that **9za** exerted significant apoptotic effect, and cellular signal pathway analysis revealed the potent blockage of phosphorylation levels of ERK and AKT in RAF-MEK-ERK and PI3K-PDK1-AKT pathways, respectively. The results reported here provide robust experimental basis for the discovery and optimization of dual pathway agents for anti-lung cancer therapy.

### Keywords

Dual inhibitor, RAF-MEK-ERK pathway, PI3K-PDK1-AKT pathway, Lung cancer, 5-(phenylamino) indolone, Structure-activity relationship;

**Abbreviations:** SAR, structure activity relationship; NSCLC, non-small-cell lung cancer; CADD, computer-aided drug design; FBDD, fragment-based drug design; MOE, molecular operating environment; H460, NCI-H460 cancer cell line; FACS, fluorescence-activated cell sorting; PI, propidium iodide; FBS, fetal bovine serum; EA, acetyl acetate; PE, petroleum ether.

\*Corresponding authors: Department of Medicinal Chemistry, Xiangya School of Pharmaceutical Sciences, Central South University, Changsha, Hunan, 410013, China

*Email address:* qbli@csu.edu.cn

## 1. Introduction

Nowadays, lung cancer becomes the second and first place in the rank of tumor morbidity and mortality, respectively<sup>1</sup>. The advance in the understanding of disease mechanism accelerates the establishment of **molecularly** targeted therapy that now has been implicated as the superior choice for cancer therapy. RAF-MEK-ERK and PI3K-PDK1-AKT pathways play pivotal roles in the process of tumor proliferation, differentiation, invasion and metastasis. Around 16% cancers show pan-RAS mutations which result in consistent phosphorylation of ERK in RAF-MEK-ERK cascade and AKT in PI3K-PDK-AKT cascade<sup>2, 3</sup>. RAF mutants exist in approximately 70% of melanoma, 100% of hairy cell leukemia and 41% of hepatocellular carcinoma. Meanwhile, PI3K mutants, such as *PIK3CA* and *PIK3IR*, have been identified as key therapeutic target in lung cancer, breast cancer and colon cancer<sup>4</sup>. RAF-MEK-ERK and PI3K-PDK1-AKT pathways are over-activated in several cancers, and they are considered as essential targets for anti-cancer drug discovery<sup>5, 6</sup>.

There are dozens of monotherapies targeting these two pathways in clinic use or clinical trial, including inhibitors that blocking BRAF (Vemurafenib and Dabrafenib), MEK (PD0325901 and Selumetinib) and PI3K (Idelalisib and Buparlisib)<sup>4, 7</sup>. However, due to the crosstalk and compensatory activation between these two pathways, monotherapy showed therapeutic efficacy which limited to 6-8 months, and in soon, acquired drug resistance occurred. Also, the strategy of combinational therapy of inhibitors targeting RAF-MEK-ERK and PI3K-PDK1-AKT pathways showed reasonable delay of acquired drug resistance, but formula composition and drug-drug interactions hinder the broad application **to a certain extent**<sup>8, 9</sup>. More specifically, the over-activation level and their relative ratio of these two pathways are heterogeneous among different patients. Moreover, such ratio might vary a lot even for a patient but at the different disease stages. Because cancer cells are so smart to evade normal therapeutics, **in together with the complexity of combinatory therapy**, alternative strategy **is** required to tackle current challenges.

Pursuing dual inhibitor of RAF-MEK-ERK and PI3K-PDK-AKT cascades has been a hot topic in the recent development of anticancer therapeutics. Ross *et al.* reported bifunctional MEK1/PI3K inhibitor **Comp. I** through conjugating a PI3K inhibitor and a MEK inhibitor via a covalent linker, which shows potent inhibitory effect on the activity of MEK1 and PI3K in enzymatic inhibition assay and significant antitumor activity in cell assay (**Figure 1**)<sup>10, 11</sup>. However, this simple covalent conjugation generates big molecular size which might pose difficulty in cell uptake, and increasing research interests are devoted in the design of small chemical scaffold. Zhang *et al.* firstly reported dual inhibitors with small scaffold, i.e., **Comp. II**. **Comp. II**, which strongly downregulate the over-activation of RAF-MEK-ERK and PI3K-PDK-AKT cascades and impede cell proliferation<sup>12</sup>. Through *in silico* screening, Park *et al.* identified **Comp. III** and **Comp. IV** from a library of 23,000 molecules. *In vitro* assay results showed the IC<sub>50</sub> value of 2.2–8.5  $\mu$ M for MEK1, and the IC<sub>50</sub> value of 0.3–10.2  $\mu$ M for PI3K $\alpha$ <sup>13</sup>. Beside these reports above, there is still a lack of diversity of chemical scaffolds to sequester the effect of synergic blockade against RAF-MEK-ERK and PI3K-PDK-AKT pathways, which could be potential as promising antitumor therapy with potential low recurrence rate.

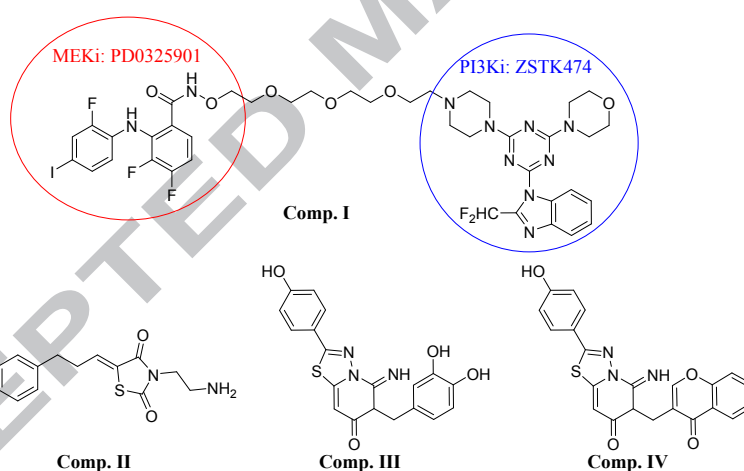


**Figure 1.** Reported dual inhibitors of RAF-MEK-ERK and PI3K-PDK-AKT pathways.

For this purpose, we reported the design on dual inhibitor of RAF-MEK-ERK and PI3K-PDK-AKT pathways and examined the efficacy as potential anticancer agents. A prototype of dual MEK/PDK1 inhibitor, 3-substituted 5-phenylamin-indolone, was settled by merging the core structural scaffolds of PD0325901 (MEK inhibitor) and BX517 (PDK1 inhibitor). Over tuning the bond property of 3-substituent on 5-phenylamin-indolone, three series of compounds in total 43 were synthesized, including 3-alkenyl (Series **I**), 3-alkyl (Series **II**), and 3-hydroxy (Series **III**). To our knowledge, this is the first report on the comparative study of three classes of 3-substituted-5-phenylamin-indolone. Moreover, a convenient and high yield synthetic method to introduce -OH group at site 3 in indolone was established. Preliminary anticancer activity and antitumor mechanism were studied in non-small cell lung cancer (NSCLC) cell lines. Structure-activity relationship (SAR) analysis revealed the

following order of antitumor activity that 3-hydroxy (Series III) > 3-alkenyl (Series I) > 3-alkyl indolone (Series II). Significantly, hit compound **9za** in Series III showed  $IC_{50}$  of  $1.8 \pm 0.8 \mu M$  in A549 cells, and further studies confirmed that **9za** exerts apoptotic effect through the blockage of ERK and AKT phosphorylation in RAF-MEK-ERK and PI3K-PDK1-AKT pathways, respectively. **9za** could be a lead scaffold as dual pathway inhibitor for the future development of anti-lung cancer agents.

## 2. Results and discussion

### 2.1. Structural Design

MEK and PDK1 are the central components in RAF-MEK-ERK and PI3K-PDK1-AKT pathways respectively. In the timeline of clinical development of MEK inhibitors, diphenylamine scaffold has been well-characterized as a activity-indispensable scaffold responsible for the binding in the allosteric site, such as PD0325901, pimasertib, selumetinib and trametinib<sup>14</sup>. BX517 is a specific PDK1 inhibitor with  $IC_{50}$  value less than 6.0 nM. It occupies the same binding site of the adenosine triphosphate (ATP) which sets up three critical Hydrogen bonds with the backbone of the hinge region<sup>15, 16</sup>.

Herein, we selected PD0325901 (MEK inhibitor) and BX517 (PDK1 inhibitor) as lead compounds and designed a prototype of dual pathway inhibitors, 3-substituted-5-phenylamin-indolone. The designed structures contain a diphenylamine scaffold for the binding to MEK allosteric pocket, and at the same time, 3-substituted-indolone scaffold was designed to preserve PDK1 inhibitory potency. Meanwhile, because bond-rotating property originating from large substituent poises critical influence on protein binding affinity, we outlined three series of compounds based on the bond variations of 3-sbustituent, i.e., 3-alkenyl-5-(phenylamino) indolone (Series I), 3-alkyl-5-(phenylamino) indolone (Series II) and 3-hydroxy-5-(phenylamino) indolone (Series III) (Figure 2).

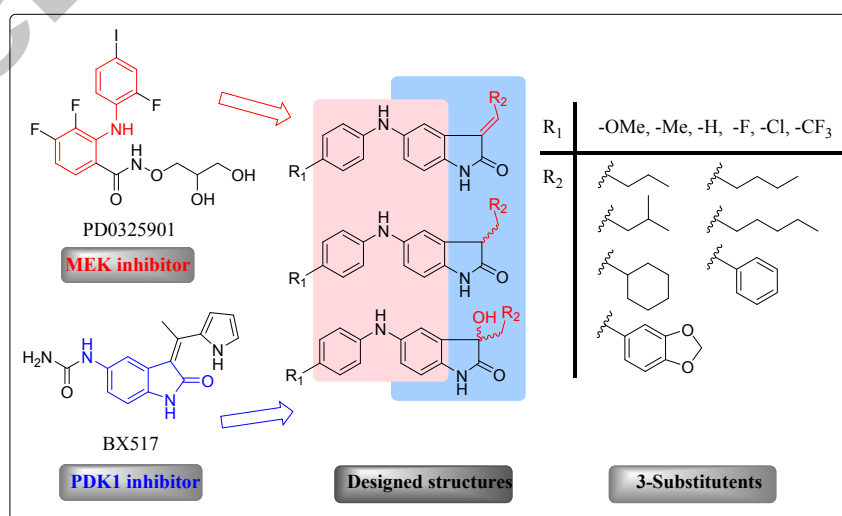


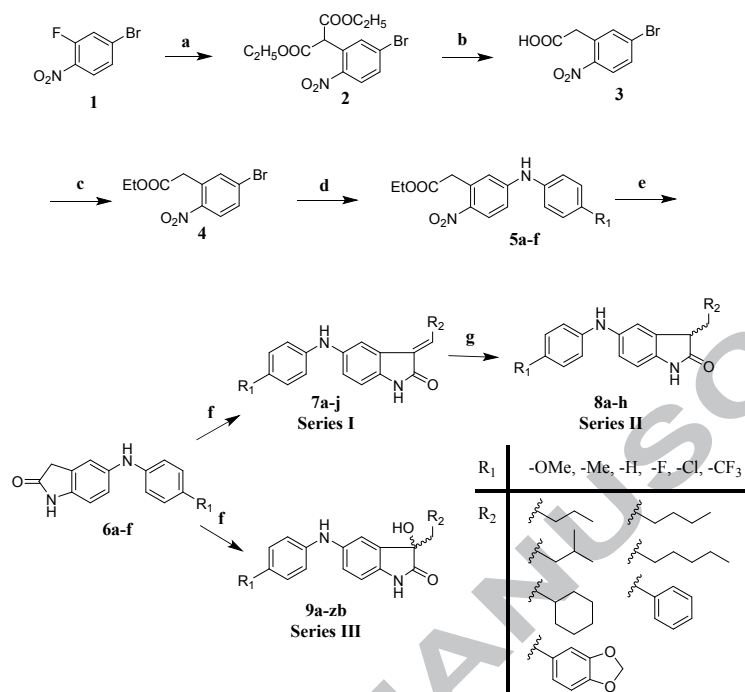
**Figure 2.** Fragment-based drug design of three series of dual inhibitors of RAF-MEK-ERK and PI3K-PDK1-AKT

pathways.

To our best knowledge, this was the first report on the comparison on three kinds of 3-substituents in one study, including 3-alkenyl, 3-alkyl and 3-hydroxy. Through literature studies, 3-alkenyl-5-(phenylamino) indolone exhibited potent anticancer activity<sup>17</sup>. After the reduction of 3-alkenyl bond into 3-alkyl-5-(phenylamino) indolone, the latter scaffold led to a significant loss on anticancer activity. Such a decrease in anticancer activity can be partially explained by the high free rotating energy of 3-alkyl bond, which causes unstable binding in the enzyme allosteric pocket<sup>17</sup>. Furthermore, the introduction of 3-hydroxy group has attracted increasing attentions in the development of potent antitumor agents, such as TMC-95A, maremycin and arundaphine<sup>18</sup>. Importantly, this research also enriched the structural diversity through introducing variable lengths of the side chain, degrees of chemical bond saturation and steric shapes at 3-substituent site.

## 2.2. Chemistry

2-fluorine-4-bromonitrobenzene (**1**) as the starting material was reacted with aniline through C-N coupling reaction catalyzed by CuI (Supplementary **S1**)<sup>19</sup>. Interestingly, it only gave substituted aniline product in high yield, which can be explained that nitro group (-NO<sub>2</sub>) strongly activates 2-F group. Of note, these unexpected results led to the development of a facile, one-pot synthetic method of 1-Phenyl-1*H*-benzimidazole derivatives facilitated by Fe, and those results have been published elsewhere (Supplementary **S2**)<sup>20</sup>. After learned this lesson, we revised the synthetic route. Diethyl malonate was firstly reacted with **1** to obtain **2** (**Scheme 1**). Followed by decarboxylation (**3**) and esterification (**4**), **4** was obtained in up to 95% yield<sup>21</sup>. Then it was coupled with various substituted phenylamines (**5**) in high yield catalyzed by Pd(PPh<sub>3</sub>)<sub>4</sub> under argon atmosphere. This reaction could not proceed using CuI/*N,N'*-dimethylethylenediamine or CuI/proline as catalysis neither in the absence nor presence of argon protection. The following step is one-pot synthesis to obtain critical intermediate **6**, through the sequential reaction of hydrogenation of -NO<sub>2</sub> group and self-cyclization of indolone heterocycle.



**Scheme 1.** Synthetic route of 5-phenylaminoindolone derivatives **7a-j** (Series I), **8a-h** (Series II) and **9a-zb** (Series III). Reagents and conditions: a. NaH, CH (COOC<sub>2</sub>H<sub>3</sub>)<sub>2</sub>, DMSO, 80-100°C; b. con. HCl, CH<sub>3</sub>COOH, 120°C; c. ethanol, 90°C; d. R<sub>1</sub>PhNH<sub>2</sub>, Pd(P(Ph)<sub>3</sub>)<sub>4</sub>, Cs<sub>2</sub>CO<sub>3</sub>, 90-110°C; e. Pd/C, H<sub>2</sub>, CH<sub>3</sub>COOH; f. RuCl<sub>3</sub>·xH<sub>2</sub>O, PPh<sub>3</sub>, NaOH, RCH<sub>2</sub>OH, 110°C, 1h for **7a-j** and 5h for **9a-zb**; g. H<sub>2</sub>, Pd/C, ethanol, rt.

There are several approaches to introduce 3-alkenyl bond at indolone scaffold by reacting with carbonyl substrates, such as piperidine/EtOH, piperidine/THF and KF/Al<sub>2</sub>O<sub>3</sub>/microwave<sup>22, 23</sup>. However, these methods obtain *cis-trans* isomer mixture. Meanwhile, there was no report on the introduction of 3-hydroxy substitution into indolone in simple way. Jensen *et al.* reported 3-alkylate substitution catalyzed by RuCl<sub>3</sub>·xH<sub>2</sub>O/PPh<sub>3</sub> (toluene, 110°C, 20 h) with a yield of 71-92%, and they proposed the formation of 3-alkenyl indolone intermediate as the reaction mechanism<sup>24</sup>. We followed their report but had minus adjustments. Intermediate **6** and benzyl alcohol were used as starting materials. At 1 h, we detected the formation of 3-alkenyl-5-(phenylamino) indolone **7** (Series I) with the yield of 85%, which is consistent with the report (Scheme 2). Through structural confirmation by <sup>1</sup>H NMR and 2D-NOSY, **Comp. 7** was identified as (*E*)-configuration. This unexpected result would expand the synthesis of conformational selective product because there is no report for the synthesis of optical pure configuration of (*E*)-3-alkenyl indolone (Supplementary S3-S4).

Furthermore, when the reaction time elongated further, **Comp.7** gradually converted to **9** instead of **8**, which is dissimilar from previous report (Scheme 1). After 5-6h, **Comp.9** reached the peak yield. When the reaction time was longer than 10 to 15 h, **9** discomposed gradually. Taken together, we

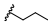
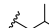
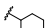
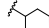
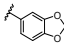
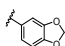
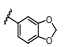
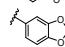
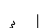




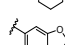
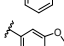
reported the synthesis of 3-hydroxy indolone catalyzed by  $\text{RuCl}_3 \cdot x\text{H}_2\text{O} \cdot \text{PPh}_3$ , using substituted indolone and organic alcohol as substrates <sup>25</sup>. All target compounds (in total 43 compounds) were structurally confirmed by HRMS,  $^1\text{H}$  NMR and  $^{13}\text{C}$  NMR, and the purities of which are higher than 95.0%.

### 2.3. Anti-proliferative activity in vitro

NSCLCs engage in approximately 85% of lung cancers, including squamous cell carcinoma, adenocarcinoma and large cell carcinoma. In spite of progresses in the combinatorial therapy of chemo- and radio-therapy, 1-year survival rate is around 44%, and the 5-year survival rate is lower than 17% <sup>26</sup>. Here, we evaluated all 43 compounds on anti-proliferative activity in two NSCLCs cell lines, A549 and NCI-H460 (H460) using MTT method <sup>27</sup>. Since most NSCLCs have been specified as adenocarcinoma, the following SAR analysis were mainly focused on antiproliferative activity in adenocarcinoma cell line A549.

Based on cell viability data shown in [Table 1](#) and [Table 2](#), SAR analysis were conducted. The electrostatic effects were firstly studied at  $\text{R}_1$  site since we intentionally introduced diverse substituents at this site. Results showed that the incorporation of electro-withdrawing group at  $\text{R}_1$  site was favorable for the anticancer activity, suggesting that preserving strong electronegative substituent at  $\text{R}_1$  site was necessary ([Figure 4A,B](#)). More specifically, in Series **I**, when  $\text{R}_2$  was cyclohexyl methylene or 3-benzodioxole-5-ylmethylene, *p*-Cl (**7f**,  $2.4 \pm 0.6$   $\mu\text{M}$ ) is 12-fold higher inhibitory activity than *p*-Me (**7b**,  $28.2 \pm 0.7$   $\mu\text{M}$ ) ([Figure 4A](#)). Similar principle was also observed in Series **II** and Series **III**. When  $\text{R}_2$  was saturate alkyl groups or different size of cyclic ring groups, the increase of electronegativity was accompanied with the enhancement of inhibitory activity ([Figure 4A,B](#)).

**Table 1.** Antiproliferative activity of Series **I** (**7a–j**) and Series **II** (**8a–h**) on A549 and H460 cell lines.

Comp.	$\text{R}_1$	$\text{R}_2$	$\text{IC}_{50} \pm \text{SD}$ ( $\mu\text{M}$ )		Comp.	$\text{R}_1$	$\text{R}_2$	$\text{IC}_{50} \pm \text{SD}$ ( $\mu\text{M}$ )	
			A549	H460				A549	H460
<b>7a</b>	<i>p</i> -Me		$3.6 \pm 1.1$	$19.0 \pm 1.7$	<b>8a</b>	<i>p</i> -Me		$6.6 \pm 0.7$	$55.3 \pm 1.4$
<b>7b</b>	<i>p</i> -Me		$28.2 \pm 0.7$	$45.5 \pm 1.1$	<b>8b</b>	<i>p</i> -Me		$>30$	$>100$
<b>7c</b>	<i>p</i> -Me		$16.7 \pm 1.0$	$>100$	<b>8c</b>	<i>p</i> -Me		$18.9 \pm 0.5$	$63.6 \pm 0.9$
<b>7d</b>	<i>p</i> -F		$26.3 \pm 0.8$	$>100$	<b>8d</b>	<i>p</i> -F		$>30$	$>100$
<b>7e</b>	<i>p</i> -Cl		$7.4 \pm 0.2$	$50.9 \pm 1.8$	<b>8e</b>	<i>p</i> -Cl		$2.0 \pm 0.3$	$48.7 \pm 1.5$
<b>7f</b>	<i>p</i> -Cl		$2.4 \pm 0.6$	$13.2 \pm 0.5$	<b>8f</b>	<i>p</i> -Cl		$16.6 \pm 0.8$	$>100$
<b>7g</b>	<i>p</i> -Cl		$15.0 \pm 0.1$	$13.5 \pm 1.7$	<b>8g</b>	<i>p</i> -Cl		$6.0 \pm 1.4$	$36.7 \pm 2.7$
<b>7h</b>	<i>p</i> -Cl		$3.1 \pm 0.4$	$24.6 \pm 1.5$	<b>MK2206</b>			$3.4 \pm 0.1$	$8.1 \pm 0.4$



AZD6244

5.2±0.3

&gt;100

**Table 2.** Antiproliferative activity of Series III (9a–zb) on A549 and H460 cell lines.

Comp.	R <sub>1</sub>	R <sub>2</sub>	IC <sub>50</sub> ±SD (μM)		Comp.	R <sub>1</sub>	R <sub>2</sub>	IC <sub>50</sub> ±SD (μM)	
			A549	H460				A549	H460
9a	<i>p</i> -OMe		8.0±1.2	16.2±0.7	9o	<i>p</i> -F		24.9±1.8	80.4±0.8
9b	<i>p</i> -OMe		18.6±0.2	>100	9p	<i>p</i> -Cl		2.8±1.1	24.4±0.7
9c	<i>p</i> -OMe		>30	>100	9q	<i>p</i> -Cl		1.9±1.2	40.8±1.4
9d	<i>p</i> -Me		7.5±0.1	31.8±1.6	9r	<i>p</i> -Cl		2.7±0.9	25.0±2.5
9e	<i>p</i> -Me		8.1±0.9	>100	9s	<i>p</i> -Cl		5.4±0.5	30.3±4.3
9f	<i>p</i> -Me		12.5±1.3	22.7±2.2	9t	<i>p</i> -Cl		3.1±2.3	20.2±2.8
9g	<i>p</i> -Me		12.1±0.7	>100	9u	<i>p</i> -Cl		3.0±0.6	26.6±6.5
9h	<i>p</i> -Me		4.1±1.0	31.6±0.3	9v	<i>p</i> -CF <sub>3</sub>		2.3±1.7	12.0±3.9
9i	<i>p</i> -Me		11.9±0.4	14.7±1.0	9w	<i>p</i> -CF <sub>3</sub>		2.2±0.6	16.3±2.9
9j	<i>p</i> -F		6.5±0.7	32.5±2.5	9x	<i>p</i> -CF <sub>3</sub>		4.2±0.7	17.2±4.6
9k	<i>p</i> -F		5.9±0.3	>100	9y	<i>p</i> -CF <sub>3</sub>		2.8±0.1	18.8±3.7
9l	<i>p</i> -F		5.7±1.6	16.8±0.6	9z	<i>p</i> -CF <sub>3</sub>		2.0±0.9	9.1±2.1
9m	<i>p</i> -F		12.0±0.5	50.7±2.8	9za	<i>p</i> -CF <sub>3</sub>		1.8±0.8	18.2±0.7
9n	<i>p</i> -F		3.0±0.6	18.1±3.5	9zb	<i>o</i> -Cl		2.3±0.2	14.6±0.9

The steric effect of substituents was widely discussed in drug development. In terms of 3-hydroxy-5-(phenylamino) indolone derivatives (Series III), the activities were negatively correlated with the steric effect of R<sub>2</sub> substituents either for saturated alkyl groups or for aromatic groups. For example, when R<sub>1</sub> is *p*-Me, the larger size of R<sub>2</sub> with both alkyl and aromatic groups showed weak inhibitory activity (Figure 4B).

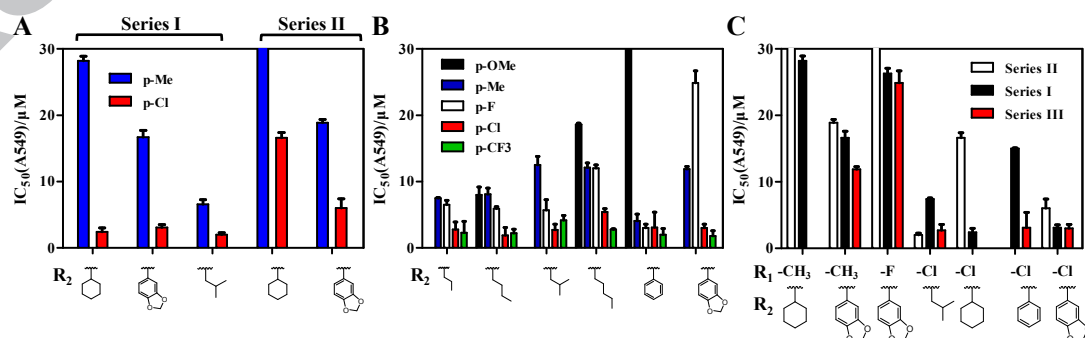


**Figure 4.** SAR analysis among three series of target products. SAR analysis of Electro-effects in para-substituents in Series I-II (A) and Series III (B). (C) Comparison study among Series I, II, and III.

As discussed in structural design, we devised three series of structures at 3-site of 5-(phenylamino) indolone, i.e. 3-alkenyl bond (Series **I**), free rotatable 3-alkyl bond (Series **II**), and 3-hydroxy (Series **III**). We wanted to study the unanimous rules of the difference among three series compounds related with anticancer activity. Expectedly, there is a significant tendency when we apply inter-series comparison. The 3-alkenyl bond in Series **I** was preferable than the freely rotated single bond in Series **II**, which contributes unfavorably to the affinity of compound towards the target molecules (Figure 4C). The underlying mechanism could be that fixed (*E*)-structure of Series **I** was in favor of the interaction with enzyme active site, while freely rotate single bond in Series **II** devastates the binding affinity<sup>17, 28</sup>. Furthermore, regarding to the introduction of 3-hydroxy group, compounds in Series **III** displayed highest inhibitory activity among three series. In consistent with computer docking study, 3-hydroxy in Series **III** was critical responsible for inhibitory effect which contact with Met219 residue through hydrogen bond interaction (Supplementary S4)<sup>18, 28</sup>. Similarly, in H460 cell lines, compounds of Series **II** exhibited lowest antiproliferative activity among whole library. Taken these data together, SAR analysis from cell viability assay in two lung cancer cell lines demonstrated the following order of antitumor activity that 3-hydroxy (Series **III**) > 3-alkenyl (Series **I**) > 3-alkyl indolone (Series **II**). In addition, we screened two hit compounds, **9q** and **9za**, with IC<sub>50</sub> of 1.9±1.2 μM and 1.8±0.8 μM respectively in A549 cells, which showed higher anti-proliferative activity than AZD6244 and MK2206.

#### 2.4. Apoptosis assay

Mechanistic study such as apoptosis assay and signaling pathway assay could help to sequester the anti-proliferative effect. Thus, apoptosis study using fluorescence-activated cell sorting (FACS) analysis was performed firstly in A549 cell lines<sup>29</sup>.

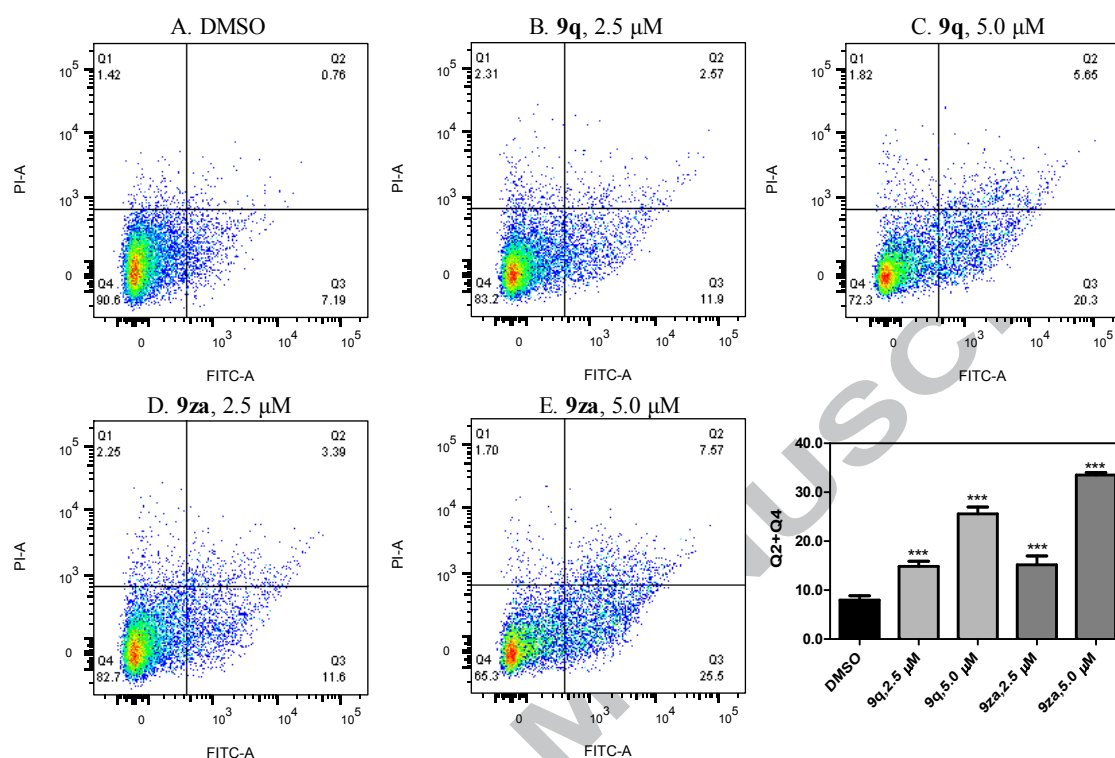


**Figure 5.** Apoptosis assay using flow cytometry on A549 cells. (A-E) Representative flow cytometry scatter plots of propidium iodide (PI) (Y axis) vs Annexin-FITC (X axis). Evaluation by Annexin V-FITC versus PI staining of A549 cells after 12 h incubation of 2.5  $\mu$ M and 5.0  $\mu$ M of **9q** and **9za**. DMSO as control group. The bottom left indicates normal cells, the bottom right indicates early apoptotic, the top right is late apoptotic and the top left is necrotic cells (numbers indicate the respective percentages of total cell populations). (F) Bar charts show quantitative data of average of three independent flow cytometry experiments in A549 cells (\* $p$  < 0.05, \*\* $p$  < 0.01 compared with control group).

According to the flow cytometric Annexin V-FITC/PI assay in A549 cells after 12 h treatment, **9q** and **9za** exert a significant increase of apoptotic cell population (**Figure 5**). At the concentration of 2.5  $\mu$ M, **9q** induced pro-apoptosis cell with population of 11.9% and necrotic cells (2.6%). After increased the concentration of **9q** to 5.0  $\mu$ M, there was similar activity on inducing apoptotic cells (20.3% pro-apoptosis and 5.7% necrotic cells). Compared with **9q** and control group, a more potent antiproliferative activity was observed with **9za** treatment. At the concentration of 2.5  $\mu$ M, the ratio of pro-apoptosis percentage was 11.6%, without obvious increase in the proportion of necrotic cells (only 3.4%). Interestingly, when the concentration of **9za** increased to 5.0  $\mu$ M, there is a significant increment of necrotic cells which took up 33.1%, with a similar level of pro-apoptosis cells (25.5%).

## 2.5. Anti-phosphorylation activity assay

To characterize the mechanism of **9za** upon inhibitory effect on RAF-MEK-ERK and PI3K-PDK1-AKT pathways, we performed kinase phosphorylation activity analysis with AZD6244 and MK2206 as positive control<sup>9</sup>. We analyzed several central cellular components in these two pathways, including p-ERK, t-ERK, p-AKT, t-AKT and  $\beta$ -actin.

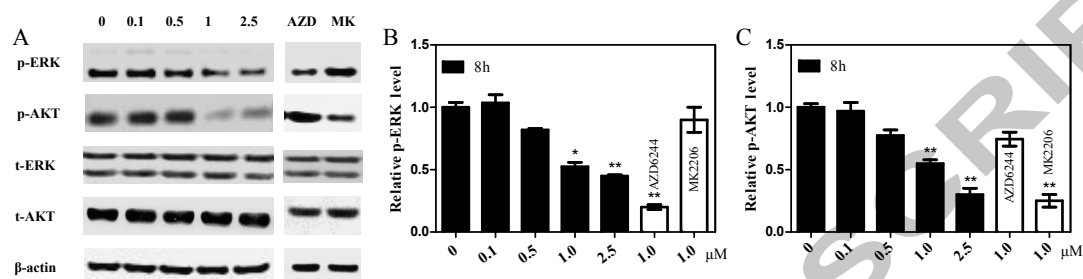


**Figure 6.** Anti-phosphorylation effect of **9za** on RAF-MEK-ERK and PI3K-PDK1-AKT pathways in A549 cells. (A) Representative western blot results of p-ERK, p-AKT, t-ERK and t-AKT.  $\beta$ -actin was included as a loading control. The band density in western blot calculated the ratio of proteins p-ERK (B) and p-AKT (C) in comparison with  $\beta$ -actin by using Image J software. Results are presented as the average of three independent experiments (\* $p$  < 0.05, \*\* $p$  < 0.01 vs control).

After 8-hour treatment, AZD6244 showed 65% inhibition of p-ERK level at 1.0  $\mu$ M with no effect on p-AKT, and MK2206 downregulated p-AKT level to 33% at 1.0  $\mu$ M which also shows slight effect on RAF-MEK-ERK pathway (Figure 6). Promisingly, **9za** inhibited both p-ERK and p-AKT level significantly in dose-dependent manner. Although the inhibitory effect of **9za** at higher concentration of 2.5  $\mu$ M is similar to AZD6244 and MK2206 at lower concentration of 1.0  $\mu$ M in p-ERK and p-AKT level, the synergic effect to block both RAF-MEK-ERK and PI3K-PDK1-AKT pathways generated more potent therapeutic effects, which might be an explanation for the higher activity of **9za** in A549 and H460 cell lines compared with AZD6244 and MK2206. These results highlighted that biological functions of the designed compounds are through down-regulation of ERK phosphorylation in RAF-MEK-ERK pathway and AKT phosphorylation in PI3K-PDK1-AKT pathway, followed by cell apoptotic effects and cell proliferative inhibition.

## 2.6. *In silico* preliminary docking study

A practical application of complex-based pharmacophore model is to determine interaction points to trigger the optimization of binding affinity and selectivity. Harnessing the knowledge about the rationality of the project design, we performed *in silico* docking study of representative compounds with MEK1 kinase and PDK1 kinase by using Molecular operating environment (MOE) software<sup>30</sup>.

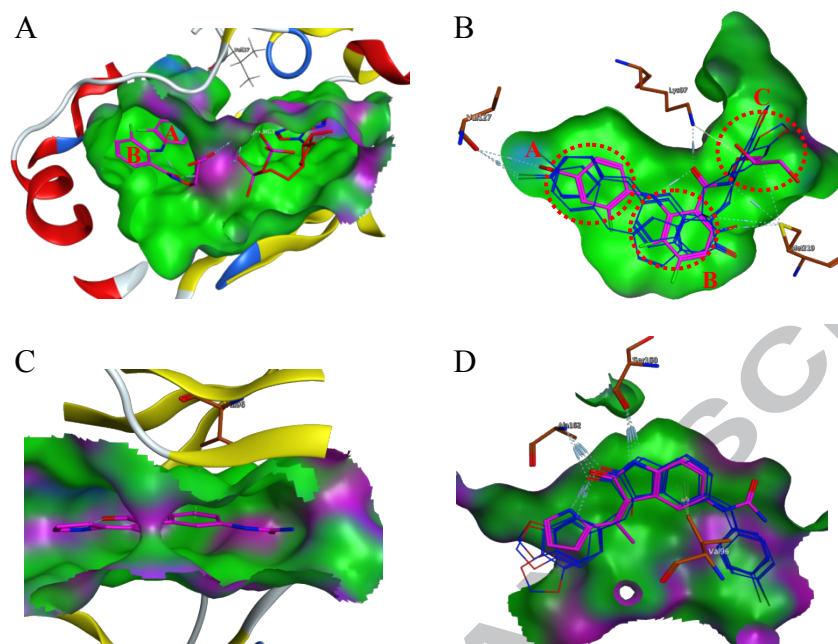


**Figure 3.** (A) The molecular docking model of PD0325901-MEK1 complexes (PDB: 3EQG)<sup>30</sup>. Left pocket shows PD0325901 (purple) in MEK1 allosteric binding site and right pocket highlights ATP (red) in ATP-binding site. A and B stand for two phenyl groups of PD0325901 respectively. (B) Docking study of three representative compounds (blue) with MEK1 allosteric binding site. A stands for 5-phenyl group, B represents central indolone scaffold, and C stands for 3-substituent. (C) The molecular docking model of BX517 (purple) binding in ATP-binding site in PDK1 (PDB: 2PE1)<sup>31</sup>. (D) Docking study of three representative structures in each series (blue) with PDK1. Before the docking study, some necessary preparatory works have been done, including water removing and hydrogen addition for protein and Powell energy gradient minimization.

PD0325901 is a non-ATP competitive inhibitor which represents one of the most potent and specific inhibitors of MEK-ERK signaling. In PD0325901-MEK1 crystal structure (**Figure 3A**) (PDB: 3EQG)<sup>30</sup>, MEK consists of ATP-binding site (right side, red color) and allosteric site (left side, purple color). The main core scaffold of PD0325901, diphenylamine localized at the center of the allosteric pocket, while the side chain of PD0325901 which lies at the inlet of this pocket, suggesting that the site chain is the favorable site for chemical modification<sup>30</sup>. Thereafter, we docked all three representative compounds into MEK1 allosteric pocket with PD0325901 in purple and design compound in blue (**Figure 3B**). As shown in the docking study, the designed structures fitted to this hydrophobic pocket in the way alike PD0325901 with interactions including Lys97, Val127 and Met219 (**Supplementary S5**). The pocket inlet was occupied with 3-substituent, and the introduction of extra interaction moiety might further enhance the binding affinity. Additionally, the forward inner space of MEK1 pocket was relatively narrow, suggesting that a larger substituent at 5-phenyl group should be avoided. Continually, based on the results of docking study on BX517-PDK1

(Figure 3C) (PDB: 2PE1)<sup>31</sup> and designed structures with PDK1 (Figure 3D), key interactions shared among designed structures and BX517 in ATP-binding site have been revealed, including Val96, Ser160 and Ala162 (supplementary S6). Indolone scaffold lay inside of the pocket, and further substitution at N-1 position might pose steric hindrance. At the same time, 3-side chain occupied inlet and substituent at 5-phenyl group centered at outlet, which imply the potential modification sites<sup>31</sup>. According to CADD studies, 3-hydroxy group as hydrogen donor might form hydrogen bond with the amino residue in the MEK allosteric pocket.

Results from docking study well explained SAR analysis and provided valuable experience for future development of dual MEK1/PDK1 enzyme inhibitor. For example, 3-side chain modifications such as introduction of hydrogen donor/acceptor would increase interaction between ligand with both MEK1 inlet and PDK1 inlet<sup>15</sup>. However, large substituents at N-1 site and large modification group at 5-phenyl group would increase steric hindrance for PDK1 complexes and MEK1 complexes respectively. Even though 9za was proved to target RAF-MEK-ERK and PI3K-PDK1-AKT dual pathway, there is still lack of direct evidence to show the specific binding to MEK1 and PDK1, and further experimental demonstration of enzyme binding activity must be required.

### 3. Conclusions

In addition to non-specific cytotoxic agents<sup>32</sup> and selective cytotoxic agents<sup>33-35</sup>, molecularly targeted therapy has become the research interests on cancer chemotherapy, especially in the era of personalized precision medicine<sup>36, 37</sup>. The over-activation of RAF-MEK-ERK and PI3K-PDK1-AKT pathways in cancer is considered as essential targets for effective cancer-targeting therapeutics. However, the monotherapy of RAF-MEK-ERK pathway inhibitor and PI3K-PDK1-AKT pathway inhibitor shows relatively short-term clinic efficacy, and mutual compensatory activations are partly responsible for the acquired resistance<sup>4</sup>. Substantial efforts have been invested on co-targeting of these two signaling pathways, which were believed to be a promising chemotherapeutic strategy in effective cancer treatment<sup>8</sup>.

In summary, we studied three prototypes of bifunctional MEK/PDK1 inhibitors by merging a MEK1 non-ATP-competitive inhibitor with a PDK1 inhibitor. Through analyzing cell viability in lung cancer cells, SAR analysis revealed the inhibitory activity order that 3-hydroxy-5-(phenylamino) indolone (Series III) > 3-alkenyl-5-(phenylamino) indolone (Series I) > 3-alkyl-5-(phenylamino) indolone (Series II). We identified lead compound 9za with IC<sub>50</sub> value of 1.8±0.8 μM in A549 cell line. Continually, mechanistic studies from flow cytometry assay and cellular signaling pathway analysis demonstrated that 9za induced cancer cell apoptosis, which was triggered by potent blockage of phosphorylation levels in RAF-MEK-ERK and PI3K-PDK1-AKT pathways. Current research should provide useful experimental results for further development of dual pathway inhibitor for targeted anticancer drug development.

## 4. Experimental

### 4.1. Chemical synthesis

#### 4.1.1. General

Reagents and solvents were purchased from standard suppliers and used without further purification. Hydrogen reduction synthesis was conducted by using BLT-2000 equipment (Beijing Jiawei Corp.). Melting point was determined on a WRS-2 melting apparatus (Shanghai YiCe Apparatus & Equipment co., LTD). Column chromatography purification was carried out on silica (80–100 mesh and 300–400 mesh). The purity of all target compounds was confirmed to be >95% by HPLC analysis conducted on an Agilent 20AT liquid chromatograph system. HPLC was carried out at room temperature using a Promosil-C18 column (250 × 4.6 mm, 5 μm) in a speed of 1 ml/min with methanol and water as **mobile phase**. The detection wavelength was set at 254 nm. <sup>1</sup>H NMR, <sup>13</sup>C NMR and 2D-NOSY spectra were recorded on Bruker AVANCE III 500MHz and 400MHz spectrometer. The chemical shifts were presented in terms of parts per million with TMS as the internal reference. In <sup>1</sup>H NMR data, *s* means single peak, *d* is double peak, *dd* is di-double peak, *t* is triple peak, *q* is quartet and *m* stands for multiple peak.

#### 4.1.2. Synthesis of key examples (full information were listed in supplementary data file)

**Diethyl 2-(5-Bromo-2-Nitrophenyl) Malonate (2).** To a solution of 20 ml n-hexane, add 5.0 g 60% NaH (125 mmol) and stir 2 min, then remove suspension. Slowly add 90 ml DMSO and 13.5 g diethyl malonate (100 mmol). Control the temperature under 40 °C. Then put mixture heated at 60 °C for 15 min and cooled down to rt. Add 11.0 g **1** (50 mmol) by drop. The mixture was heated at 80 °C for 4.5 h and then cooled to rt. Add 100 ml saturated NH<sub>4</sub>Cl solution to stop the reaction. Three times extraction with acetyl acetate (EA) were performed and washed with saturated NaCl solution, then dry with Na<sub>2</sub>SO<sub>4</sub>. Remove EA by evaporation and obtained 17.9 g Diethyl 2-(5-Bromo-2-Nitrophenyl) Malonate (**2**) and proceed to next step without purification. Yellow solid, yield: 99.0%, mp. 70–72°C, HPLC: 99.1%. HRMS (ESI) *m/z* calcd for [C<sub>13</sub>H<sub>14</sub>BrNO<sub>6</sub>+H]<sup>+</sup> 381.9902; found, 381.9901 [M+Na]<sup>+</sup>, 383.9882 [M+Na]<sup>+</sup>.

**5-Bromo-2-Nitrophenylacetic acid (3).** To a solution of 60 ml 6 N HCl and 60 ml AcOH, dissolve 17.9 g **2** (50 mmol) and stir at 110 °C overnight. Remove all solvent and obtain 12.5 g 5-Bromo-2-Nitrophenylacetic acid (**3**), mp. 174.4–175.9 °C, yield 98%. Intermediate **3** proceed to next step without further purification. To a solution of 100 ml dehydrated EtOH and 0.5 ml conc. H<sub>2</sub>SO<sub>4</sub>, add 12.9 g **3** (50 mmol).

**Ethyl 2-(5-Bromo-2-Nitrophenyl)Acetate (4).** Put the mixture in oil bath and reflux overnight. Cool down to rt and place at -5 °C overnight until the total precipitation occurred. Filtrate white precipitate and obtain 12.5 Ethyl 2-(5-Bromo-2-Nitrophenyl)Acetate (**4**), yield 99.2%. White solid, mp. 50.5–52.8 °C, HPLC: 98.5%. <sup>1</sup>H NMR (300 MHz,



DMSO- $d_6$ )  $\delta$ : 8.06 (dd,  $J$  = 8.7, 3.3 Hz, 1H, Ar-H), 7.93 – 7.72 (m, 2H, Ar-H), 4.08 (d,  $J$  = 2.9 Hz, 4H), 1.22 – 1.08 (m, 3H).  $^{13}\text{C}$  NMR (75 MHz, DMSO- $d_6$ )  $\delta$ : 169.42, 136.17, 132.22, 131.70, 127.42, 126.80, 60.60, 38.29, 13.97.

**Ethyl 2-(2-nitro-5-(p-tolylamino)phenyl)acetate (5b).** To a 100 ml three neck bottle, add 2.9 g **4** (10 mmol), 6.5 g  $\text{Cs}_2\text{CO}_3$  (20 mmol), 0.11 g  $\text{Pd}(\text{PPh}_3)_4$  (1 mmol), 45 ml DMF, and 1.4 g p-tolylamine (15 mmol). Ar protection and heated at 90 °C for 5 h. Cool down to rt, stop the reaction with 70 ml  $\text{H}_2\text{O}$ . Adjust pH to 5.0–6.0 with 6 N HCl. Followed by EA extraction, sat. NaCl washing, and  $\text{Na}_2\text{SO}_4$  drying. Obtain 2.78 g Ethyl 2-(2-nitro-5-(p-tolylamino)phenyl)acetate (**5b**). Proceed to next step without further purification. Yellow solid, yield: 98.2%, mp. 76.4–77.2°C, HPLC: 98.2%.  $^1\text{H}$  NMR (500 MHz,  $\text{CDCl}_3$ )  $\delta$ : 8.14 (d,  $J$  = 9.1 Hz, 1H), 7.28 (s, 1H), 7.21 (d,  $J$  = 8.0 Hz, 2H), 7.15 – 7.07 (m, 2H), 6.84 (dd,  $J$  = 9.1, 2.6 Hz, 1H), 6.69 (d,  $J$  = 2.6 Hz, 1H), 4.20 (q,  $J$  = 7.1 Hz, 2H), 3.95 (s, 2H), 2.38 (s, 3H), 1.29 (td,  $J$  = 7.1, 2.1 Hz, 3H).  $^{13}\text{C}$  NMR (100 MHz,  $\text{CDCl}_3$ )  $\delta$ : 170.31, 149.96, 139.28, 136.59, 134.86, 133.40, 130.31, 128.54, 122.75, 117.46, 112.57, 61.10, 41.13, 20.93, 14.19.

**Ethyl 2-(2-Nitro-5-(Phenylamino)Phenyl)Acetate (5c).** Synthetic method refers to **5b**. Yellow solid, yield: 97.2%, mp. 74.5–76.1°C, HPLC: 97.2%.  $^1\text{H}$  NMR (300 MHz, DMSO- $d_6$ )  $\delta$ : 9.26 (s, 1H), 8.16 – 8.04 (m, 1H, Ar-H), 7.37 (dd,  $J$  = 13.4, 7.1 Hz, 2H, Ar-H), 7.25 (d,  $J$  = 6.6 Hz, 2H, Ar-H), 7.09 (dd,  $J$  = 12.9, 6.6 Hz, 1H, Ar-H), 7.05 – 6.93 (m, 2H, Ar-H), 4.14 – 3.90 (m, 4H), 1.24 – 1.07 (m, 3H).  $^{13}\text{C}$  NMR (75 MHz, DMSO- $d_6$ )  $\delta$ : 169.95, 149.69, 140.06, 138.02, 133.57, 129.45, 128.09, 123.26, 120.68, 117.52, 112.62, 60.16, 40.28, 14.05. HRMS (ESI)  $m/z$  calcd for  $[\text{C}_{16}\text{H}_{16}\text{N}_2\text{O}_4+\text{H}]^+$  300.1110; found, 301.1184  $[\text{M}+\text{H}]^+$ .

**Ethyl 2-(2-nitro-5-(p-tolylamino)phenyl)acetate (6b)**

To a hydrogen reduction equipment, add 2.86 g **5b** (10 mmol), 0.14 g 10% Pd/C, and 45 ml AcOH. Stir overnight at rt under the atmosphere of 0.4 MPa  $\text{H}_2$ . Filtrate and recycle Pd/C. Remove solvent and perform silica column purification with 200–300 mesh silica. Mobile phase is petroleum ether (PE): EA 2:1. Obtain 1.9 g Ethyl 2-(2-nitro-5-(p-tolylamino)phenyl)acetate (**6b**). White solid, yield: 85.2%, mp. 194.5–196.1°C, HPLC: 97.2%.  $^1\text{H}$  NMR (500 MHz,  $\text{CDCl}_3$ )  $\delta$ : 8.44 (s, 1H), 7.08 (d,  $J$  = 8.1 Hz, 2H), 7.02 (s, 1H), 6.92 (dd,  $J$  = 15.0, 5.3 Hz, 3H), 6.80 (d,  $J$  = 8.3 Hz, 1H), 5.49 (s, 1H), 3.53 (s, 2H), 2.31 (s, 3H). HRMS (ESI)  $m/z$  calcd for  $[\text{C}_{14}\text{H}_{12}\text{N}_2\text{O}+\text{H}]^+$  239.1184; found, 239.1189  $[\text{M}+\text{H}]^+$ .

**5-(Phenylamino)Indolin-2-One (6c).** Synthetic method refers to **6b**. White solid, yield: 87.8%, mp. 185.5–186.6°C, HPLC: 98.2%.  $^1\text{H}$  NMR (300 MHz, DMSO- $d_6$ )  $\delta$ : 10.21 (s, 1H), 7.84 (s, 1H), 7.16 (t,  $J$  = 7.9 Hz, 2H, Ar-H), 7.00 (s, 1H, Ar-H), 6.92 (d,  $J$  = 7.7 Hz, 3H, Ar-H), 6.71 (t,  $J$  = 7.9 Hz, 2H, Ar-H), 3.44 (s, 2H).  $^{13}\text{C}$  NMR (75 MHz, DMSO- $d_6$ )  $\delta$ : 176.09, 145.07, 137.51, 137.11, 129.03, 126.74, 118.27, 118.09, 116.34, 114.97, 109.41, 36.08. HRMS (ESI)  $m/z$  calcd for  $[\text{C}_{14}\text{H}_{12}\text{N}_2\text{O}+\text{H}]^+$  224.0950; found, 247.0848  $[\text{M}+\text{Na}]^+$ .

**(E)-3-Butylidene-5-(p-tolylamino)indolin-2-one (7a).** To a 50 ml three neck flask, add 0.26 g **6a** (1 mmol), 0.15 g  $\text{PPh}_3$  (0.4 mmol), 40 mg NaOH (1 mmol), 42 mg  $\text{RuCl}_3 \cdot \text{H}_2\text{O}$  (0.2 mmol), and 15 ml toluene. Mixture well and add 0.3



g n-Butyl alcohol (5 mmol). Reflux at 110 °C for 5.5 h under the protection of Ar. Then add H<sub>2</sub>O to stop the reaction, and extract with CH<sub>2</sub>Cl<sub>2</sub>, then washed by sat. NaCl and dried by Na<sub>2</sub>SO<sub>4</sub> for 5 h. Remove solvent and purified with 200-300 mesh silica column. Obtain 0.27 g (*E*)-3-Butylidene-5-(*p*-tolylamino)indolin-2-one (**7a**). Red solid, yield: 82.2%, mp. 166.1-168.2°C, HPLC: 98.7%. <sup>1</sup>H NMR (500 MHz, DMSO-*d*<sub>6</sub>) δ: 10.25 (s, 1H), 7.78 (s, 1H), 7.30 (d, *J* = 1.4 Hz, 1H, Ar-H), 7.00 (d, *J* = 8.2 Hz, 2H, Ar-H), 6.95 (dd, *J* = 8.3, 1.9 Hz, 1H, Ar-H), 6.89 – 6.85 (m, 2H, Ar-H), 6.80 – 6.72 (m, 2H, Ar-H), 2.55 (q, *J* = 7.5 Hz, 2H), 2.20 (s, 3H), 1.65 – 1.55 (m, 2H), 0.97 (t, *J* = 7.4 Hz, 3H). <sup>13</sup>C NMR (125 MHz, DMSO-*d*<sub>6</sub>) δ: 168.45, 142.69, 140.68, 138.39, 136.08, 130.03, 129.27, 127.88, 123.28, 119.01, 116.20, 114.95, 110.53, 30.88, 21.93, 20.68, 14.30. HRMS (ESI) *m/z* calcd for [C<sub>19</sub>H<sub>20</sub>N<sub>2</sub>O+H]<sup>+</sup> 293.1654; found, 293.1627 [M+H]<sup>+</sup>.

**(*E*)-3-(Cyclohexylmethylene)-5-(*p*-tolylamino)indolin-2-one (7b).**

Synthetic method refers to **7a**. Red solid, yield: 89.5%, mp. 172.4-173.5°C, HPLC: 99.2%. <sup>1</sup>H NMR (400 MHz, DMSO-*d*<sub>6</sub>) δ: 10.25 (s, 1H), 7.82 (s, 1H), 7.27 (d, *J* = 1.8 Hz, 1H, Ar-H), 7.01 (d, *J* = 8.3 Hz, 2H, Ar-H), 6.94 (dd, *J* = 8.3, 2.1 Hz, 1H, Ar-H), 6.89 (d, *J* = 8.4 Hz, 2H, Ar-H), 6.74 (d, *J* = 8.3 Hz, 1H, Ar-H), 6.59 (d, *J* = 9.5 Hz, 1H), 2.79 (d, *J* = 9.8 Hz, 1H), 2.21 (s, 3H), 1.75 (dd, *J* = 20.0, 11.6 Hz, 4H), 1.67 (d, *J* = 10.3 Hz, 1H), 1.42 – 1.20 (m, 5H). <sup>13</sup>C NMR (100 MHz, DMSO-*d*<sub>6</sub>) δ: 168.72, 145.22, 142.46, 138.56, 135.94, 130.02, 128.01, 127.68, 122.78, 118.85, 116.39, 114.25, 110.64, 37.74, 31.65, 25.75, 25.57, 20.70. HRMS (ESI) *m/z* calcd for [C<sub>22</sub>H<sub>24</sub>N<sub>2</sub>O+H]<sup>+</sup> 333.1967; found, 333.1959 [M+H]<sup>+</sup>.

**(*E*)-3-(Benzo[*d*][1,3]dioxol-5-ylmethylene)-5-(*p*-tolylamino)indolin-2-one (7c).**

Synthetic method refers to **7a**. Red solid, yield: 86.5%, mp. 175.1-175.8°C, HPLC: 97.5%. <sup>1</sup>H NMR (500 MHz, DMSO-*d*<sub>6</sub>) δ: 10.34 (s, 1H), 7.75 (s, 1H), 7.49 (s, 1H), 7.43 (d, *J* = 2.0 Hz, 1H), 7.30 – 7.22 (m, 2H), 7.03 – 6.99 (m, 3H), 6.90 (dd, *J* = 8.3, 2.1 Hz, 1H), 6.83 (dd, *J* = 7.7, 5.9 Hz, 2H), 6.76 (d, *J* = 8.3 Hz, 1H), 6.10 (s, 2H), 2.20 (d, *J* = 5.9 Hz, 3H). <sup>13</sup>C NMR (125 MHz, DMSO-*d*<sub>6</sub>) δ: 169.26, 148.89, 148.06, 142.20, 138.27, 136.62, 136.07, 130.03, 128.79, 127.96, 127.38, 124.77, 122.01, 120.08, 116.54, 112.25, 111.02, 109.70, 109.11, 102.04, 20.71. HRMS (ESI) *m/z* calcd for [C<sub>23</sub>H<sub>18</sub>N<sub>2</sub>O<sub>3</sub>+H]<sup>+</sup> 371.1396; found, 371.13940[M+H]<sup>+</sup>.

**3-Isopentyl-5-(*p*-tolylamino)indolin-2-one (8a).** To a hydrogen reduction equipment, add 0.17 g **7a** (0.5 mmol), 10 mg 10% Pd/C, and EtOH. Stir 1.5 h at rt under the atmosphere of 0.4 MPa H<sub>2</sub>. Filtrate and recycle Pd/C. Remove solvent and perform silica column purification with 200-300 mesh silica. Mobile phase is PE: EA 2:1. Obtain 1.7 g 3-Isopentyl-5-(*p*-tolylamino)indolin-2-one (**8a**). White solid, yield: 99.1%, mp. 185.1-185.8°C, HPLC: 98.5%. <sup>1</sup>H NMR (500 MHz, DMSO-*d*<sub>6</sub>) δ: 10.16 (s, 1H), 7.72 (s, 1H), 6.97 (d, *J* = 7.8 Hz, 3H, Ar-H), 6.86 (dd, *J* = 13.7, 5.1 Hz, 3H, Ar-H), 6.71 (d, *J* = 8.2 Hz, 1H, Ar-H), 2.19 (s, 3H), 1.89 – 1.71 (m, 2H), 1.48 (dt, *J* = 13.2, 6.6 Hz, 1H), 1.14 – 1.07 (m, 2H), 0.83 (d, *J* = 6.6 Hz, 6H). <sup>13</sup>C NMR (125 MHz, DMSO-*d*<sub>6</sub>) δ: 179.09, 142.88, 138.34, 136.55, 131.15, 129.96, 127.66, 117.64, 116.05, 115.67, 109.93, 45.94, 34.60, 28.16, 27.97, 22.85, 20.66. HRMS (ESI) *m/z* calcd for

$[\text{C}_{20}\text{H}_{24}\text{N}_2\text{O}+\text{H}]^+$  309.1967; found, 309.1943  $[\text{M}+\text{H}]^+$ .

**3-(Cyclohexylmethyl)-5-(p-tolylamino)indolin-2-one (8b).** Synthetic method refers to **8a**. Red solid, yield: 98.4%, mp. 171.2-172.8°C, HPLC: 97.5%.  $^1\text{H}$  NMR (500 MHz, DMSO)  $\delta$ : 10.15 (s, 1H), 7.74 (s, 1H), 7.00 (t,  $J = 11.0$  Hz, 2H, Ar-H), 6.93 (s, 1H, Ar-H), 6.90 – 6.81 (m, 3H, Ar-H), 6.71 (d,  $J = 8.2$  Hz, 1H, Ar-H), 3.42 (dt,  $J = 13.6, 4.1$  Hz, 1H), 2.20 (s, 3H), 1.76 – 1.51 (m, 8H), 1.21 – 1.11 (m, 3H), 0.95 – 0.85 (m, 2H).  $^{13}\text{C}$  NMR (125 MHz, DMSO- $d_6$ )  $\delta$ : 179.55, 142.80, 138.25, 136.23, 131.59, 129.97, 127.70, 117.42, 116.10, 115.82, 109.97, 43.59, 38.27, 34.65, 33.54, 32.84, 26.49, 26.27, 26.17, 20.68. HRMS (ESI)  $m/z$  calcd for  $[\text{C}_{22}\text{H}_{26}\text{N}_2\text{O}+\text{H}]^+$  335.2123; found, 335.2100  $[\text{M}+\text{H}]^+$ .

**3-(Benzo[d][1,3]dioxol-5-ylmethyl)-5-(p-tolylamino)indolin-2-one (8c).** Synthetic method refers to **8a**. Red solid, yield: 99.2%, mp. 194.5-195.8°C, HPLC: 98.5%.  $^1\text{H}$  NMR (500 MHz, DMSO- $d_6$ )  $\delta$ : 10.16 (s, 1H), 7.64 (s, 1H), 6.96 (d,  $J = 8.2$  Hz, 2H, Ar-H), 6.77 (dd,  $J = 7.7, 3.2$  Hz, 3H, Ar-H), 6.73 (d,  $J = 8.3$  Hz, 2H, Ar-H), 6.67 – 6.62 (m, 3H, Ar-H), 5.93 (d,  $J = 4.5$  Hz, 2H), 3.73 (dd,  $J = 8.1, 5.0$  Hz, 1H), 3.23 (dd,  $J = 13.9, 4.9$  Hz, 1H), 2.81 (dd,  $J = 13.9, 8.5$  Hz, 1H), 2.20 (d,  $J = 4.4$  Hz, 3H).  $^{13}\text{C}$  NMR (125 MHz, DMSO- $d_6$ )  $\delta$ : 178.37, 147.46, 146.08, 142.72, 138.09, 136.32, 132.42, 130.27, 129.94, 129.88, 127.54, 122.76, 118.14, 116.05, 115.74, 110.05, 109.82, 108.36, 101.12, 77.25, 47.25, 35.62, 20.68. HRMS (ESI)  $m/z$  calcd for  $[\text{C}_{23}\text{H}_{20}\text{N}_2\text{O}_3+\text{H}]^+$  373.1552; found, 373.1526  $[\text{M}+\text{H}]^+$ , 395.1340  $[\text{M}+\text{Na}]^+$ .

**3-(Benzo[d][1,3]dioxol-5-ylmethyl)-5-(4-fluorophenylamino)indolin-2-one (8d).** Synthetic method refers to **8a**. Red solid, yield: 99.5%, mp. 195.2-197.1°C, HPLC: 97.5%.  $^1\text{H}$  NMR (500 MHz, DMSO- $d_6$ )  $\delta$ : 10.19 (s, 1H), 7.75 (s, 1H), 6.99 (dd,  $J = 15.2, 6.3$  Hz, 2H, Ar-H), 6.78 (td,  $J = 8.7, 4.1$  Hz, 5H, Ar-H), 6.64 (dd,  $J = 20.3, 7.6$  Hz, 3H, Ar-H), 5.93 (s, 2H), 3.73 (dd,  $J = 8.2, 5.0$  Hz, 1H), 3.23 (dd,  $J = 13.9, 4.9$  Hz, 1H), 2.81 (dd,  $J = 13.9, 8.4$  Hz, 1H).  $^{13}\text{C}$  NMR (125 MHz, DMSO- $d_6$ )  $\delta$ : 178.39, 147.45, 146.07, 141.92, 137.79, 136.77, 132.41, 130.37, 122.78, 118.57, 116.97, 116.91, 116.14, 116.00, 115.82, 110.13, 109.84, 108.37, 101.12, 47.26, 35.55. HRMS (ESI)  $m/z$  calcd for  $[\text{C}_{22}\text{H}_{17}\text{FN}_2\text{O}_3+\text{H}]^+$  377.1301; found, 377.1270  $[\text{M}+\text{H}]^+$ .

**3-Hydroxy-5-(4-methoxyphenylamino)-3-pentylindolin-2-one (9a).** The main difference of synthesis with Series I is longer reaction time, which elongate from 1.5 h to 5.5 h. More specifically, to a 50 ml three neck flask, add 0.26 g **6a** (1 mmol), 0.15 g  $\text{PPh}_3$  (0.4 mmol), 40 mg NaOH (1 mmol), 42 mg  $\text{RuCl}_3 \cdot \text{H}_2\text{O}$  (0.2 mmol), and 15 ml toluene. Mixture well and add 0.3 g n-Butyl alcohol (5 mmol). Reflux at 110 °C for 5.5 h under the protection of Ar. Then add  $\text{H}_2\text{O}$  to stop the reaction, and extract with  $\text{CH}_2\text{Cl}_2$ , then washed by sat. NaCl and dried by  $\text{Na}_2\text{SO}_4$  for 5 h. Remove solvent and purified with 200-300 mesh silica column. Obtain 0.27 g 3-Hydroxy-5-(4-methoxyphenylamino)-3-pentylindolin-2-one (**9a**). White solid, yield: 75.1%, mp. 192.6-194.3°C, HPLC: 97.9%.  $^1\text{H}$  NMR (400 MHz, DMSO- $d_6$ )  $\delta$ : 9.98 (s, 1H), 7.63 (s, 1H), 6.94 (t,  $J = 6.3$  Hz, 3H, Ar-H), 6.70 – 6.77 (m, 3H, Ar-H), 6.68 (t,  $J = 13.7$  Hz, 1H, Ar-H), 5.76 (s, 1H), 3.71 (s, 3H), 1.79 – 1.64 (m, 2H), 1.26 – 1.11 (m, 6H), 1.12 – 0.90 (m, 2H), 0.85 (t,  $J = 6.8$  Hz, 3H).  $^{13}\text{C}$  NMR (100 MHz, DMSO- $d_6$ )  $\delta$ : 179.99, 153.45, 139.96, 138.19, 134.53, 133.58, 118.87, 116.87, 115.02,

113.89, 110.30, 76.45, 55.69, 38.37, 31.55, 29.22, 23.16, 22.39, 14.35. HRMS (ESI)  $m/z$  calcd for  $[C_{20}H_{24}N_2O_3+H]^+$  341.1865; found, 341.1414  $[M+H]^+$ .

**3-Hexyl-3-hydroxy-5-(4-methoxyphenylamino)indolin-2-one (9b).** Synthetic method refers to **9a**. White solid, yield: 76.4%, mp. 174.9-178.1°C, HPLC: 96.0%.  $^1H$  NMR (400 MHz, DMSO- $d_6$ )  $\delta$ : 9.99 (s, 1H), 7.61 (s, 1H), 6.92 (t,  $J$  = 6.3 Hz, 3H, Ar-H), 6.88 – 6.77 (m, 3H, Ar-H), 6.67 (t,  $J$  = 13.7 Hz, 1H, Ar-H), 5.76 (s, 1H), 3.69 (s, 3H), 1.76 – 1.62 (m, 2H), 1.24 – 1.11 (m, 6H), 1.09 – 0.90 (m, 2H), 0.81 (t,  $J$  = 6.8 Hz, 3H).  $^{13}C$  NMR (100 MHz, DMSO- $d_6$ )  $\delta$ : 179.63, 153.44, 139.93, 138.19, 134.50, 133.58, 118.87, 116.87, 115.02, 113.89, 110.30, 76.45, 55.69, 38.37, 31.53, 29.22, 23.16, 22.39, 14.35. HRMS (ESI)  $m/z$  calcd for  $[C_{21}H_{26}N_2O_3+H]^+$  355.2021; found, 355.2013  $[M+H]^+$ .

**3-Benzyl-3-hydroxy-5-(4-methoxyphenylamino)indolin-2-one (9c).** Synthetic method refers to **9a**. White solid, yield: 81.2%, mp. 194.3- 195.4°C, HPLC: 95.33%.  $^1H$  NMR (400 MHz, DMSO- $d_6$ )  $\delta$ : 9.87 (s, 1H), 7.55 (s, 1H), 7.20 – 7.10 (m, 3H, Ar-H), 7.05 – 6.93 (m, 2H, Ar-H), 6.87 – 6.78 (m, 4H, Ar-H), 6.77 (d,  $J$  = 2.2 Hz, 1H, Ar-H), 6.71 (dd,  $J$  = 8.2, 2.3 Hz, 1H, Ar-H), 6.50 (d,  $J$  = 8.2 Hz, 1H, Ar-H), 6.05 (s, 1H), 3.70 (s, 3H), 3.18 – 2.87 (m, 2H).  $^{13}C$  NMR (100 MHz, DMSO- $d_6$ )  $\delta$ : 179.13, 153.30, 139.48, 138.29, 135.78, 134.55, 132.29, 130.66, 128.03, 126.76, 118.62, 117.86, 115.00, 114.51, 110.28, 77.27, 55.71, 44.04. HRMS (ESI)  $m/z$  calcd for  $[C_{22}H_{20}N_2O_3+H]^+$  361.1552; found, 361.1546  $[M+H]^+$ .

**3-Butyl-3-hydroxy-5-(*p*-tolylamino)indolin-2-one (9d).** Synthetic method refers to **9a**. White solid, yield: 74.5%, mp. 212.3-213.7°C, HPLC: 95.5%.  $^1H$  NMR (500 MHz, DMSO- $d_6$ )  $\delta$ : 10.03 (s, 1H), 7.77 (s, 1H), 6.99 (dd,  $J$  = 7.9, 5.1 Hz, 3H, Ar-H), 6.93 – 6.83 (m, 3H, Ar-H), 6.69 (d,  $J$  = 8.2 Hz, 1H, Ar-H), 5.80 (s, 1H), 2.20 (s, 3H), 1.80 – 1.67 (m, 2H), 1.26 – 1.15 (m, 2H), 1.09 – 0.89 (m, 2H), 0.79 (t,  $J$  = 7.3 Hz, 3H).  $^{13}C$  NMR (125 MHz, DMSO- $d_6$ )  $\delta$ : 179.68, 142.63, 138.74, 135.18, 133.56, 130.00, 127.87, 118.30, 116.28, 115.15, 110.30, 76.42, 38.14, 25.50, 22.79, 20.68, 14.34. HRMS (ESI)  $m/z$  calcd for  $[C_{19}H_{22}N_2O_2+H]^+$  311.1759; found, 293.1647  $[M-HO]^+$ , 311.1751  $[M+H]^+$ , 333.1570  $[M+Na]^+$ .

**3-Hydroxy-3-pentyl-5-(*p*-tolylamino)indolin-2-one (9e).** Synthetic method refers to **9a**. White solid, yield: 69.5%, mp. 192.8-194.2°C, HPLC: 96.7%.  $^1H$  NMR (400 MHz, DMSO- $d_6$ )  $\delta$ : 10.02 (s, 1H), 7.75 (s, 1H), 6.99 (d,  $J$  = 8.4 Hz, 3H, Ar-H), 6.86 (t,  $J$  = 9.8 Hz, 3H, Ar-H), 6.68 (d,  $J$  = 7.9 Hz, 1H, Ar-H), 5.78 (s, 1H), 2.20 (s, 3H), 1.69 (d,  $J$  = 7.0 Hz, 2H), 1.13 (d,  $J$  = 32.9 Hz, 4H), 1.02 (d,  $J$  = 36.1 Hz, 2H), 0.78 (s, 3H).  $^{13}C$  NMR (100 MHz, DMSO- $d_6$ )  $\delta$ : 179.67, 142.65, 138.72, 135.18, 133.54, 129.99, 127.85, 118.36, 116.27, 115.14, 110.30, 76.42, 38.29, 31.79, 22.85, 22.34, 20.68, 14.25. HRMS (ESI)  $m/z$  calcd for  $[C_{20}H_{24}N_2O_2+H]^+$  325.1916; found, 307.1806  $[M-HO]^+$ , 325.1908  $[M+H]^+$ , 347.1726  $[M+Na]^+$ .

**3-Hydroxy-3-isopentyl-5-(*p*-tolylamino)indolin-2-one (9f).** Synthetic method refers to **9a**. White solid, yield: 71.3%, mp. 223.7-225.5°C, HPLC: 94.9%.  $^1H$  NMR (400 MHz, DMSO- $d_6$ )  $\delta$ : 10.02 (s, 1H), 7.77 (s, 1H), 7.00 (s, 1H, Ar-H), 6.99 – 6.95 (m, 2H, Ar-H), 6.87 (dd,  $J$  = 7.7, 5.3 Hz, 3H, Ar-H), 6.69 (d,  $J$  = 8.2 Hz, 1H, Ar-H), 5.79 (s, 1H),

2.20 (s, 3H), 1.80 – 1.64 (m, 2H), 1.41 (dt,  $J = 13.2, 6.6$  Hz, 1H), 1.03 – 0.82 (m, 2H), 0.84 – 0.75 (m, 6H).  $^{13}\text{C}$  NMR (100 MHz, DMSO- $d_6$ )  $\delta$ : 179.62, 142.67, 138.69, 135.21, 133.49, 129.99, 127.84, 118.43, 116.21, 115.18, 110.32, 76.42, 36.26, 32.22, 28.10, 22.92, 22.86, 20.68. HRMS (ESI)  $m/z$  calcd for  $[\text{C}_{20}\text{H}_{24}\text{N}_2\text{O}_2+\text{H}]^+$  325.1916; found, 307.1806  $[\text{M}-\text{HO}]^+$ , 325.1909  $[\text{M}+\text{H}]^+$ , 347.1727  $[\text{M}+\text{Na}]^+$ .

#### 4.2. Cell line and culture conditions

A549 cells and H460 cells were purchased from ATCC (Manassas, USA). Cells were cultured in DMEM medium (Invitrogen) supplemented with 10% fetal bovine serum (FBS) and 10 mg/ml antibiotics (penicillin and streptomycin) at 37°C with 5%  $\text{CO}_2$  in humidified air. All other chemicals were purchased from Sigma-Aldrich.

#### 4.3. Anti-proliferative activity assay

$2 \times 10^5$  monocytes were seeded into the 96-well plate containing 200  $\mu\text{L}$  of culture medium<sup>38</sup>. The compounds were then individually added to the plates at 30 minutes after seeding. Plates were incubated at 37°C in 5%  $\text{CO}_2$  for 48 hours. At 4 hours before the end of incubation time, 20  $\mu\text{L}$  3-(4, 5-dimethylthiazol-2-yl)-2,5-diphenyltetrazolium bromide solution (MTT, Sigma-Aldrich, 5 mg/ml) was added to each well. After 4 hours of incubation, plates were centrifuged and culture medium was removed. Precipitated formazan crystals were dissolved by adding 200  $\mu\text{L}$  DMSO to each well. The microplates were shaken at room temperature for 10 minutes and prepared for reading using a microplate reader at the **absorption wavelength of 570 nm**. Statistical analysis was performed by using two-way analysis of variance and Tukey multiple comparison posttests with significance of  **$p$  value less than 0.05**.

#### 4.4. Apoptosis analysis

Cancer cell apoptosis was detected by flow cytometry via the examination of altered plasma membrane phospholipid packed with lipophilic dye Annexin V-FITC<sup>38</sup>. Briefly, treated cells were harvested by trypsin, washed twice with PBS, and then **re-suspended** in binding buffer at a concentration of  $1 \times 10^6$  cells/mL according to the manufacturer's instruction. Thereafter, 5  $\mu\text{L}$  of Annexin V-FITC and 5  $\mu\text{L}$  of **propidium iodide (PI) solution** were added into 100  $\mu\text{L}$  of cell suspension and incubated for 30 minutes at room temperature in the dark. **After the addition of 400  $\mu\text{L}$  of binding buffer**, labeled cells were counted by flow cytometry. All apoptotic cells at the early stage (Annexin V-FITC-positive, PI-negative), necrotic/late apoptotic cells (double positive), as well as living cells (double negative) were counted by flow cytometer and subsequently analyzed by Cell Quest software (Becton Dickinson). Argon laser excitation wavelength was 488 nm, whereas emission data were acquired at wavelength 530 nm (FL-1 channel) for FITC and 670 nm (FL-3 c3 channel) for PI.

#### 4.5. Western blot

Western blot assay was performed by following the manufactural procedure<sup>38</sup>. Primary antibody was added in BSA and allowed to incubate overnight at 4°C. After washed with TBS/0.05% Tween-20, secondary antibody was added, and then incubated for an additional 1 hour at room temperature. The membrane was again washed 3 times before adding Pierce Super Signal chemiluminescent substrate (Rockford, IL) and then immediately imaged on Chemi Doc (Bio-Rad, Hercules). The films were scanned using EPSON PERFECTION V500 PHOTO and quantified by Image J.

#### 4.6. Molecular docking

To get insight into the enzyme-compound interaction, flexible docking of ligand and protein binding pocket was performed using Molecular operating environment (MOE, 2017 version). The crystal structures of MEK1-PD0325901 (PDB ID 3EQG, 2.5 Å) and PDK1-BX-517 complexes (PDB ID 2PE1, 2.14 Å) were obtained from Protein Data Bank as the docking receptor<sup>30, 31</sup>. The 3D structures of the test set compounds were constructed using MOE builder tool and were energetically minimized via MOE energy minimization algorithm [Gradient: 0.05, Force Field: MMFF94X]. The predicted interactions of complex protein–ligand complexes were analyzed.

#### 4.7. Statistical analysis.

GraphPad prism 5.0 was used for data analysis. Results for continuous variations presented as the mean  $\pm$  standard error. Two-group differences in continuous variations were assessed by the unpaired *t*-test. *P*-values are two-tailed with confidence intervals of 95%.

### Acknowledgment

This work was supported by the National Natural Science Foundation of China (No. 21102184, 81773640), the Specialized Research Fund for the Doctoral Program of Higher Education of China (No. 20110162120033), and Natural Science Foundation of Hunan Province (No. 2016JJ2162). Hunan Province Strategic Emerging Industry Science and Technology Key Project, NO. 2016GK4028. Key research and development project of Hainan Province (project number: ZDYF2017092), Haikou, China. We also would like to thank the Nuclear Magnetic Resonance Laboratory of Advanced Research Center in Central South University for the technological assistance in chemical characterization.

### A. Supplementary data

Supplementary data associated with this article can be found online at <https://doi.org/10.1016/j.bmc.2019.xx.xxxx>.

## References

1. Siegel RL, Miller KD, Jemal A. Cancer statistics, 2018, *CA: Cancer J. Clin.* 2018;68:7-30. <http://doi.org/10.3322/caac.21442>.
2. Prior IA, Lewis PD, Mattos C. A comprehensive survey of Ras mutations in cancer, *Cancer Res.* 2012;72:2457-2467. <http://doi.org/10.1158/0008-5472>.
3. Mendoza MC, Er EE, Blenis J. The Ras-ERK and PI3K-mTOR Pathways: Cross-talk and Compensation, *Trends Biochem. Sci.* 2011;36:320-328. <http://doi.org/10.1016/j.tibs.2011.03.006>.
4. Yu Z, Ye S, Hu G, Lv M, et al. The RAF-MEK-ERK pathway: targeting ERK to overcome obstacles to effective cancer therapy, *Future Med. Chem.* 2015;7:269-289. <http://doi.org/10.4155/fmc.14.143>.
5. Hrustanovic G, Olivas V, Pazarentzos E, Tulpule A, et al. RAS-MAPK dependence underlies a rational polytherapy strategy in EML4-ALK-positive lung cancer, *Nat. Med.* 2015;21:1038-1047. <http://doi.org/10.1038/nm.3930>.
6. McCarroll JA, Gan PP, Erlich RB, Liu M, et al. TUBB3/betaIII-tubulin acts through the PTEN/AKT signaling axis to promote tumorigenesis and anoikis resistance in non-small cell lung cancer, *Cancer Res.* 2015;75:415-425. <http://doi.org/10.1158/0008-5472>.
7. Houede N, Pourquier P. Targeting the genetic alterations of the PI3K-AKT-mTOR pathway: its potential use in the treatment of bladder cancers, *Pharmacol. Ther.* 2015;145:1-18. <http://doi.org/10.1016/j.pharmthera.2014.06.004>.
8. Temraz S, Mukherji D, Shamseddine A. Dual Inhibition of MEK and PI3K Pathway in KRAS and BRAF Mutated Colorectal Cancers, *Int. J. Mol. Sci.* 2015;16:22976-22988. <http://doi.org/10.3390/ijms160922976>.
9. Meng J, Dai B, Fang B, Bekele BN, et al. Combination treatment with MEK and AKT inhibitors is more effective than each drug alone in human non-small cell lung cancer in vitro and in vivo, *PLoS One* 2010;5:e14124. <http://doi.org/10.1371/journal.pone.0014124>.
10. Van Dort ME, Hong H, Wang H, Nino CA, et al. Discovery of Bifunctional Oncogenic Target Inhibitors against Allosteric Mitogen-Activated Protein Kinase (MEK1) and Phosphatidylinositol 3-Kinase (PI3K), *J. Med. Chem.* 2016;59:2512-2522. <http://doi.org/10.1021/acs.jmedchem.5b01655>.
11. Van Dort ME, Galbán S, Nino CA, Hong H, et al. Structure-Guided Design and Initial Studies of a Bifunctional MEK/PI3K Inhibitor (ST-168), *ACS Med. Chem. Lett.* 2017. <http://doi.org/10.1021/acsmedchemlett.7b00111>.

12. Li Q, Wu J, Zheng H, Liu K, et al. Discovery of 3-(2-aminoethyl)-5-(3-phenyl-propylidene)-thiazolidine-2,4-dione as a dual inhibitor of the Raf/MEK/ERK and the PI3K/Akt signaling pathways, *Bioorg. Med. Chem. Lett.* 2010;20:4526-4530. <http://doi.org/10.1016/j.bmcl.2010.06.030>.
13. Park H, Lee S, Hong S. Discovery of MEK/PI3K dual inhibitor via structure-based virtual screening, *Bioorg. Med. Chem. Lett.* 2012;22:4946-4950. <http://doi.org/doi.org/10.1016/j.bmcl.2012.06.041>.
14. Zhao Y, Adjei AA. The clinical development of MEK inhibitors, *Nat. Rev. Clin. Oncol.* 2014;11:385-400. <http://doi.org/10.1038/nrclinonc.2014.83>.
15. Islam I, Brown G, Bryant J, Hrvatin P, et al. Indolinone based phosphoinositide-dependent kinase-1 (PDK1) inhibitors. Part 2: optimization of BX-517, *Bioorg. Med. Chem. Lett.* 2007;17:3819-3825. <http://doi.org/10.1016/j.bmcl.2007.05.060>.
16. Sestito S, Daniele S, Nesi G, Zappelli E, et al. Locking PDK1 in DFG-out conformation through 2-oxo-indole containing molecules: Another tools to fight glioblastoma, *Eur. J. Med. Chem.* 2016;118:47-63. <http://doi.org/10.1016/j.ejmech.2016.04.003>.
17. Prakash CR, Raja S. Indolinones as Promising Scaffold as Kinase Inhibitors: A Review, *Mini-Rev. Med. Chem.* 2012;12:98-119. <http://doi.org/10.2174/138955712798995039>.
18. Peddibhotla S. 3-Substituted-3-hydroxy-2-oxindole, an emerging new scaffold for drug discovery with potential anti-cancer and other biological activities, *Curr. Bioact. Compd.* 2009;5:20-38. <http://doi.org/10.2174/157340709787580900>.
19. Surry DS, Buchwald SL. Diamine Ligands in Copper-Catalyzed Reactions, *Chem Sci* 2010;1:13-31. <http://doi.org/10.1039/C0SC00107D>.
20. Yu Z, Wang Z, Wu X, Hu G, et al. "One-Pot" Synthesis of 1-Phenyl-1H-benzimidazole Derivatives Facilitated by Fe, *Chin. J. Org. Chem.* 2016;36:1672. <http://doi.org/10.6023/cjoc201512007>.
21. Albaugh P, Fan Y, Mi Y, Sun F, et al. Discovery of GNF-5837, a Selective TRK Inhibitor with Efficacy in Rodent Cancer Tumor Models, *ACS Med. Chem. Lett.* 2012;3:140-145. <http://doi.org/10.1021/ml200261d>.
22. Lee HJ, Lim JW, Yu J, Kim JN. An expedient synthesis of 3-alkylideneoxindoles by Ti(OiPr)<sub>4</sub>/pyridine-mediated Knoevenagel condensation, *Tetrahedron Lett.* 2014;55:1183-1187. <http://doi.org/10.1016/j.tetlet.2013.12.097>.
23. Chouhan M, Sharma R, Nair VA. Cp<sub>2</sub>ZrCl<sub>2</sub>-induced Reformatsky and Barbier reactions on isatins: an efficient synthesis of 3-substituted-3-hydroxyindolin-2-ones, *Appl. Organomet. Chem.* 2011;25:470-475. <http://doi.org/10.1002/aoc.1789>.
24. Jensen T, Madsen R. Ruthenium-Catalyzed Alkylation of Oxindole with Alcohols, *J. Org. Chem.* 2009;74:3990-3992. <http://doi.org/10.1021/Jo900341w>.



25. Grigg R, Whitney S, Sridharan V, Keep A, et al. Iridium catalysed C-3 alkylation of oxindole with alcohols under solvent free thermal or microwave conditions, *Tetrahedron* 2009;65:4375-4383. <http://doi.org/10.1016/j.tet.2009.03.065>.
26. Siegel RL, Miller KD, Jemal A. Cancer statistics, 2017, *CA: Cancer J. Clin.* 2017;67:7-30. <http://doi.org/10.3322/caac.21387>.
27. Yu Z, Taniguchi J, Wei Y, Pandian GN, et al. Antiproliferative and apoptotic activities of sequence-specific histone acetyltransferase inhibitors, *Eur. J. Med. Chem.* 2017;138:320-327. <http://doi.org/10.1016/j.ejmech.2017.06.037>.
28. Ai J, Lv M, Li X, Chen Z, et al. Synthesis, anti-lung cancer activity and molecular docking study of 3-methylene-2-oxindoline-5-carboxamide derivatives, *Med. Chem. Res.* 2018;27:161-170. <http://doi.org/10.1007/s00044-017-2050-3>.
29. Su Q, Peng M, Zhang Y, Xu W, et al. Quercetin induces bladder cancer cells apoptosis by activation of AMPK signaling pathway, *Am. J. Cancer Res.* 2016;6:498-508. <http://doi.org/eCollection2016>.
30. Fischmann TO, Smith CK, Mayhood TW, Myers JE, et al. Crystal Structures of MEK1 Binary and Ternary Complexes with Nucleotides and Inhibitors, *Biochemistry* 2009;48:2661-2674. <http://doi.org/10.1021/bi801898e>.
31. Islam I, Bryant J, Chou YL, Kochanny MJ, et al. Indolinone based phosphoinositide-dependent kinase-1 (PDK1) inhibitors. Part 1: design, synthesis and biological activity, *Bioorg. Med. Chem. Lett.* 2007;17:3814-3818. <http://doi.org/10.1016/j.bmcl.2007.04.071>.
32. Ralhan R, Kaur J. Alkylating agents and cancer therapy, *Expert Opin. Ther. Pat.* 2007;17:1061-1075. <http://doi.org/10.1517/13543776.17.9.1061>.
33. Morita K, Suzuki K, Maeda S, Matsuo A, et al. Genetic regulation of the RUNX transcription factor family has antitumor effects, *J. Clin. Invest.* 2017;127:2815-2828. <http://doi.org/10.1172/JCI91788>.
34. Oronsky BT, Reid T, Knox SJ, Scicinski JJ. The Scarlet Letter of Alkylation: A Mini Review of Selective Alkylating Agents, *Transl. Oncol.* 2012;5:226-229. <http://doi.org/10.1593/tlo.12187>.
35. Yu Z, Pandian GN, Hidaka T, Sugiyama H. Therapeutic gene regulation using pyrrole-imidazole polyamides, *Adv. Drug Del. Rev.* 2019;accepted. <http://doi.org/10.1016/j.addr.2019>.
36. Hood L, Friend SH. Predictive, personalized, preventive, participatory (P4) cancer medicine, *Nat. Rev. Clin. Oncol.* 2011;8:184. <http://doi.org/10.1038/nrclinonc.2010.227>.
37. Aronson SJ, Rehm HL. Building the foundation for genomics in precision medicine, *Nature* 2015;526:336. <http://doi.org/10.1038/nature15816>.
38. Peng M, Huang Y, Tao T, Peng CY, et al. Metformin and gefitinib cooperate to inhibit bladder cancer growth via both AMPK and EGFR pathways joining at Akt and Erk, *Sci.*



Rep. 2016;6:28611. <http://doi.org/10.1038/srep28611>.

# Graphic

